frontiers in Earth Science

ORIGINAL RESEARCH
published: 03 February 2022
doi: 10.3389/feart.2021.790999

Change in Subduction Dip Angle of the Indian Continental Lithosphere Inferred From the Western Himalayan Eclogites

Si Chen[1,2], *Yi Chen*[1,3]*, *Stéphane Guillot*[4] *and Qiuli Li*[1,3]

[1]State Key Laboratory of Lithospheric Evolution, and Institutions of Earth Science, Institute of Geology and Geophysics, Chinese Academy of Sciences, Beijing, China, [2]Key Laboratory of Marine Mineral Resources, Ministry of Natural Resources, Guangzhou Marine Geological Survey, Guangzhou, China, [3]College of Earth and Planetary Sciences, University of Chinese Academy of Sciences, Beijin, China, [4]University Grenoble Alpes, University Savoie Mont-Blanc, CNRS, IRD, IFSTTAR, ISTerre, Grenoble, France

OPEN ACCESS

Edited by:
Oliver Jagoutz,
Massachusetts Institute of Technology, United States

Reviewed by:
Xiao-Ping Xia,
Guangzhou Institute of Geochemistry (CAS), China
Andy Parsons,
University of Plymouth, United Kingdom

***Correspondence:**
Yi Chen
chenyi@mail.iggcas.ac.cn

Specialty section:
This article was submitted to Petrology, a section of the journal Frontiers in Earth Science

Received: 07 October 2021
Accepted: 16 December 2021
Published: 03 February 2022

Citation:
Chen S, Chen Y, Guillot S and Li Q (2022) Change in Subduction Dip Angle of the Indian Continental Lithosphere Inferred From the Western Himalayan Eclogites. Front. Earth Sci. 9:790999. doi: 10.3389/feart.2021.790999

The occurrence of ultrahigh-pressure (UHP) and high-pressure (HP) rocks in the Himalayan orogen has been conventionally attributed to the different subduction dip angles along the strike. The western Himalayan UHP eclogites point to a steep continental subduction in the Eocene. The present-day geophysical data show low subduction dip angles of the Indian lithosphere beneath southern Tibet and Karakoram, implying that a shift from steep to low-angle subduction probably happened in the western Himalaya. However, the timing and mechanism of such a subduction-angle change are still unknown. Here we present a combined analysis of zircon geochronology and geochemistry of eclogites and gneiss in the Stak massif, western Himalaya. Metamorphic zircons equilibrated with garnet and omphacite show flat heavy rare earth element patterns without Eu anomalies and, thus, yield similar eclogite-facie ages of ca. 31 Ma. The Stak HP eclogite-facie metamorphism is at least 15 Ma younger than those measured in the western Himalayan UHP eclogites, but broadly contemporaneous with other Himalayan HP rocks. Therefore, all the Himalayan HP rocks record higher peak geothermal gradients and younger ages than those of the UHP rocks. Our new data, combined with the magmatic lull observed in the Kohistan–Ladakh–Gangdese arc and with the convergent rate of the Indian plate, suggest a change in subduction dip angle over time. Consequently, we suggest that the entire Indian continental lithosphere experienced an approximately coherent shift from steep to low-angle subduction after the breakoff of the Neo-Tethyan slab since the middle Eocene. This critical change in subduction geometry is interpreted to be responsible for the transition from continental subduction to collision dynamics.

Keywords: Himalaya, Stak, eclogites, zircon chronology, subduction dip angle

INTRODUCTION

The Indo–Asia collision after the closure of the Neo-Tethys produced the present-day largest ongoing continent–continent collisional orogen of the Earth, the Himalayan orogen (Yin, 2006). Because subduction angle, convergence rate, and slab rollback/breakoff strongly influence the spatial and temporal distribution of metamorphic and magmatic rocks (Kay and Coira, 2009; Paterson and Ducea, 2015), the subduction style of the orogen can be revealed by studying these aspects.

High-pressure (HP) metamorphic rocks (blueschist, eclogite, HP granulite facies rocks, and HP garnet amphibolite facies rocks) are exposed along the Himalayan orogen (**Figure 1**). However, ultrahigh-pressure (UHP) eclogites only occur at Kaghan and Tso Morari in the western syntaxis (O'Brien et al., 2001; Sachan et al., 2004). The UHP eclogites in the western Himalaya were subducted earlier (53–46 Ma) and exhumed faster (45–40 Ma) than the HP rocks (buried at 38–15 Ma and exhumed at 25–13 Ma) in the central and eastern Himalaya (Parrish et al., 2006; Zhang et al., 2010; Donaldson et al., 2013; Rehman, 2019; Wang et al., 2021), possibly reflecting different subduction dip angles or depths of the Indian continental slab along strike (Guillot et al., 2008). Therefore, it is proposed that the Indo–Asia plates in the western syntaxis collided earlier followed by steep subduction, and that those in the central and eastern Himalaya collided later with low-angle subduction (Chemenda et al., 2000; Guillot et al., 2008; Zhang et al., 2015). Numerical models imply that a subduction angle decreases over time due to continental lithosphere buoyancy (Duretz and Gerya, 2013; Magni et al., 2017). Geophysical data point to the present-day low subduction angles (or underthrusting) of the Indian continental lithosphere beneath east and west Tibet and Karakoram (Hazarika et al., 2017; Parsons et al., 2020). If correct, the Indian continental slab underwent a shift from steep subduction to low-angle subduction or underthrusting in the western Himalaya. However, such a subduction-angle change has not been evidenced by the rocks in this region, making the timing and mechanism of such a process poorly resolved.

In addition to UHP eclogites, HP eclogites were discovered in the Stak massif in the western syntaxis (Le Fort et al., 1997). These HP–UHP eclogites record clockwise *P-T* paths (Wilke et al., 2010; Lanari et al., 2013; St-Onge et al., 2013) and, thus, define a large HP-UHP province (Guillot et al., 2008; Lanari et al., 2013). However, the Stak eclogite suffered a greater degree of overprint and recorded younger metamorphic zircon ages of 32 Ma (Kouketsu et al., 2016) than the UHP eclogites with peak metamorphic ages of 53–46 Ma (e.g., Rehman, 2019). Is this a reflection of zircon recrystallization during exhumation in Stak, or a real age of eclogite formation? It remains uncertain whether the western Himalayan HP–UHP eclogites were formed synchronously at different subducting depths and then experienced different exhumation histories or were formed by diachronous subduction of various continental slices.

Here we show, based on petrology, zircon geochronology, and geochemistry, that both the Stak eclogites and their country gneiss share the same peak metamorphic age of ca. 31 Ma. This age is younger than that of the UHP eclogites, but coeval to a magmatic lull in the entire Himalayan orogen. Steep subduction of the continental lithosphere, driven by downgoing oceanic lithosphere, would generate UHP metamorphism in the subducting crust (**Figure 2A**). However,

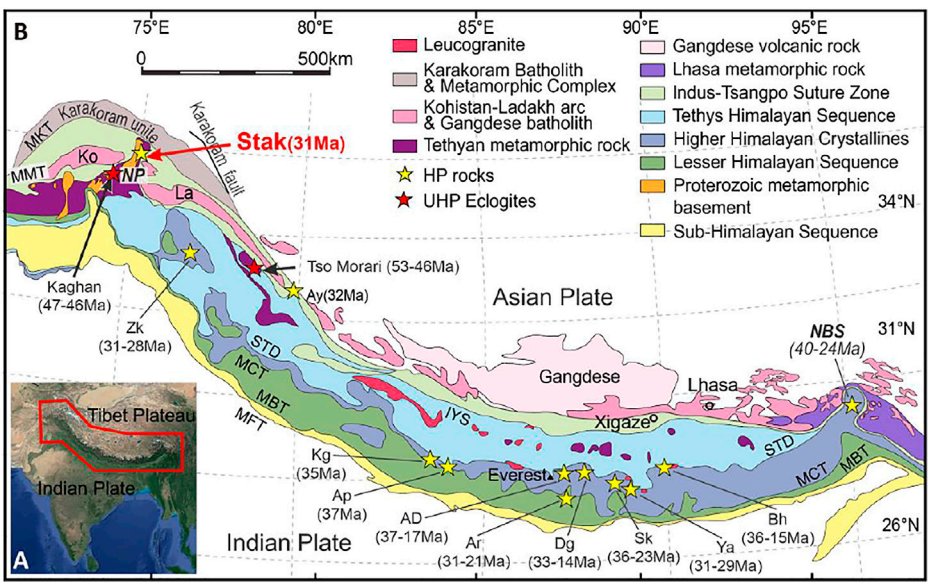

FIGURE 1 | (A) Location of the Himalayan orogen. **(B)** Geological map of Himalaya (modified after Ding et al., 2016a; Guillot et al., 2008) with locations and peak metamorphic ages of high-pressure (HP) and ultrahigh-pressure (UHP) metamorphic rocks. MKT, Main Karakoram Thrust; MMT, Main Mantle Thrust; IYS, Indus–Yarlung Suture; STD, South Tibetan Detachment; MCT, Main Central Thrust; MBT, Main Boundary Thrust; MFT, Main Frontal Thrust; AD, Ama Drime; Ap, Annapurna; Ar, Arun; Ay, Ayilari; Bh, Bhutan; Dg, Dinggye; Kg, Kali Gandaki; Ko, Kohistan arc unite; La, Ladakh arc unite; NBS, Namche Barwa Syntaxis; NPS, Nanga Parbat Syntaxis; Sk, Sikkim; Ya, Yadong; Zk, Zanskar. Detailed age data and sources are listed in **Supplementary Table S6**.

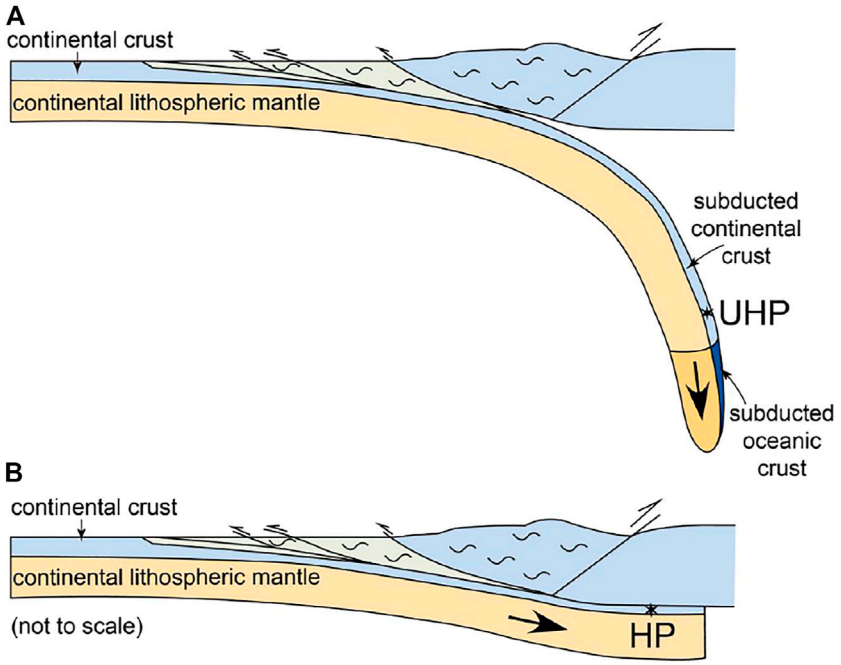

FIGURE 2 | Schematic diagrams showing the relation between subduction angle and metamorphism. **(A)** Steep subduction of continental lithosphere triggered by downgoing oceanic lithosphere would produce UHP metamorphism. **(B)** Low-angle (shallow) subduction leads to the underthrusting of continental lithosphere producing HP metamorphism.

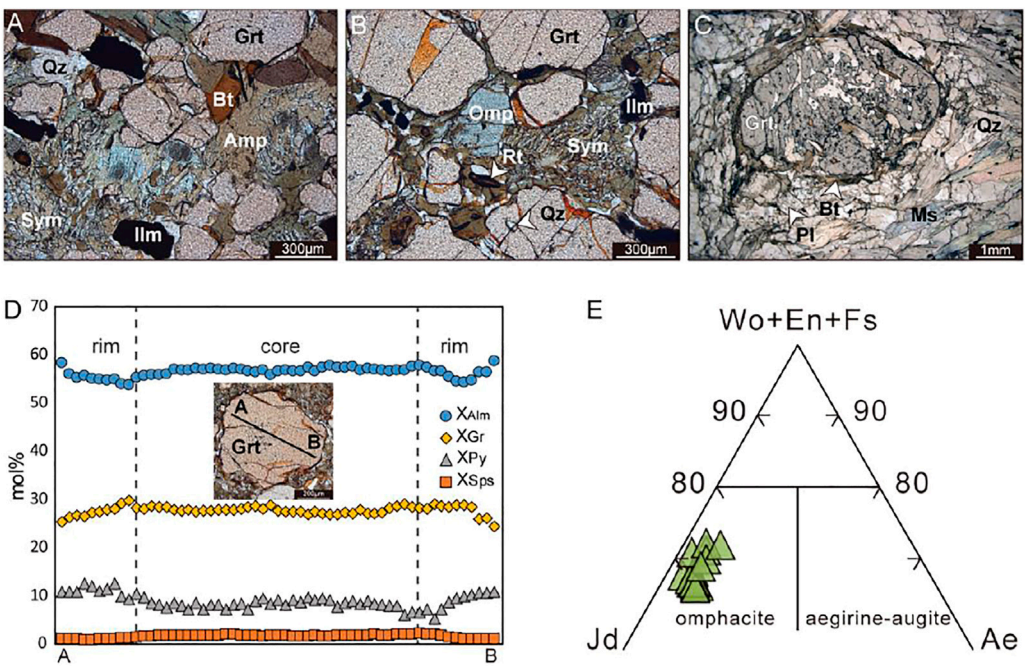

FIGURE 3 | Photomicrographs of the eclogites 16PK190 **(A)** and 16PK194 **(B)**, and gneiss 16PK181 **(C)**. **(D)** Zoning profile of a garnet in the eclogite 16PK194. **(E)** Ternary diagram showing the composition of omphacite in eclogite. Mineral abbreviations are after Whitney and Evans (2010).

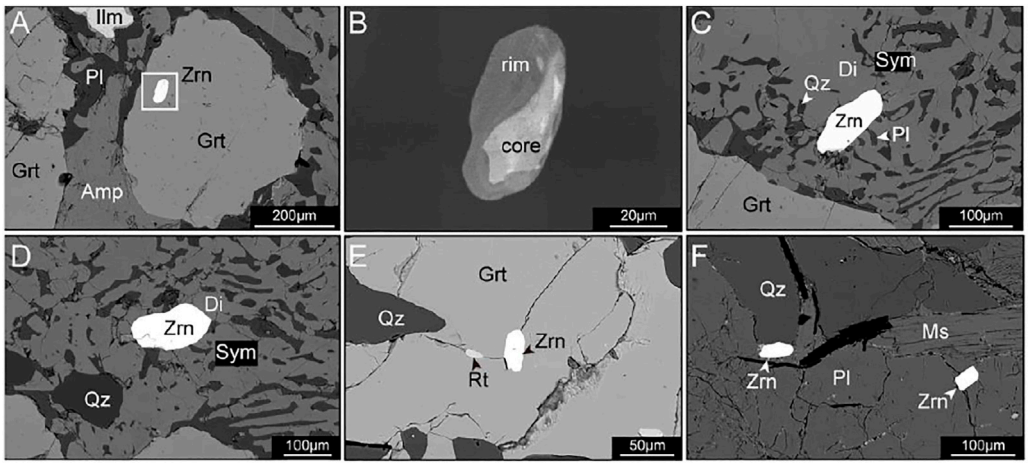

FIGURE 4 | Back-scattered electron (BSE) images showing microstructure of zircon in eclogites **(A,C,D)** and gneiss **(E,F)**; **(B)** Cathodoluminescence (CL) image of zircon inclusion in garnet enlarged for the square of **(A)**.

the continental lithosphere, without driven force from subducted oceanic lithosphere, would undergo low-angle subduction or underthrusting (Magni et al., 2017) and, thus, more likely produce HP metamorphism (**Figure 2B**). Based on geological and geophysical records, we further infer a uniform change in the subduction dip angle over 2,500 km throughout the Himalayan belt since the middle Eocene.

GEOLOGICAL SETTING AND SAMPLES

The Stak massif is located in the north Indian continental margin, northeast of the Nanga Parbat–Haramosh massif (NPHM), southwest of the Ladakh arc (**Figure 1B**), and close to the Main Mantle Thrust (MMT). This massif consists of gneisses, schists, metabasites, with minor marbles, and develops fold and imbricate structures (Guillot et al., 2008). Eclogites with extensive retrogression in the Stak massif occur as boudins or dikes in the gneisses. A detailed petrological study on the Stak eclogites yields HP peak conditions at ~750°C and ~2.5 GPa and retrograde conditions at 650°C–700°C and 0.9–1.6 GPa (Lanari et al., 2013). This retrograde temperature is slightly higher than those (<600°C at 1.0–1.7 GPa) of the Kaghan and Tso Morari UHP eclogites (Wilke et al., 2010; Wilke et al., 2015).

The peak metamorphic age of the Stak eclogite is still unknown. Sensitive high-resolution ion microprobe (SHRIMP) zircon U-Pb data yielded scattered ages between 70 and 50 Ma (Riel et al., 2008). However, Kouketsu et al. (2016) used the same method to show that a small cluster of low Th/U (<0.03) and Yb (<10 ppm) zircon ages are concentrated between 36 and 28 Ma with a lower intercept age of ~32 Ma. This age was interpreted as recrystallization after eclogite-facie metamorphism, which was possibly induced by heating from nearby NPHM at lower crustal levels (Kouketsu et al., 2016).

The present study focuses on the eclogite boudins (16PK190 and 16PK194) and country gneiss (16PK181) in the Stak massif. Both eclogite samples contain an eclogite-facies assemblage of garnet, omphacite, quartz, and rutile (**Figure 3**). Garnet is surrounded by amphibole and plagioclase kelyphite and has a compositionally homogeneous core ($Alm_{55–57}Prp_{7–13}Grs_{24–28}Sps_{1–2}$) (see the **Supplementary Table S1**) with a narrow retrograde zoning rim. Omphacite with a 23.4–30.0 mol.% jadeite component (**Supplementary Table S2**) is partially replaced by fine-grained symplectite of diopside + plagioclase + amphibole. The symplectite is rimmed by coarser (200–500 μm) amphibole and biotite. The eclogite sample zircons occur as inclusions within garnet and symplectite, and as an intergranular phase in the matrix (**Figure 4**). The zircon grains in the symplectite are larger (~100 μm) than the plagioclase and diopside grains, and show disequilibrium texture with these phases. The gneiss (16PK181) contains garnet, muscovite, biotite, plagioclase, and quartz with minor rutile and zircon (**Figure 3**). The garnet is surrounded by plagioclase and mica, and could be a relict eclogite-facie phase. The gneiss sample zircons exist as matrix phases and inclusions within garnet and muscovite (**Figure 4**).

MATERIALS AND METHODS

Mineral Major Elements

Major elements of rock-forming minerals were analyzed using an electron microprobe analyzer (EPMA, JEOL-JXA8100) at the IGG-CAS. The operating conditions were a 15-kV accelerating voltage, a 20-nA beam current, and 3-μm spot diameter. The counting time was 20 s at peak and 10 s at the lower and upper background positions, respectively. All data were corrected online using a modified ZAF (atomic number, absorption, and fluorescence) correction procedure. The detection limits (1σ) were in the range of 0.008–0.02wt%. The precision of the major element analysis was better than 1.0%.

Zircon U-Pb Isotopes and Trace Elements

Zircon grains were separated from samples by using conventional heavy liquid and magnetic separation techniques. Approximately

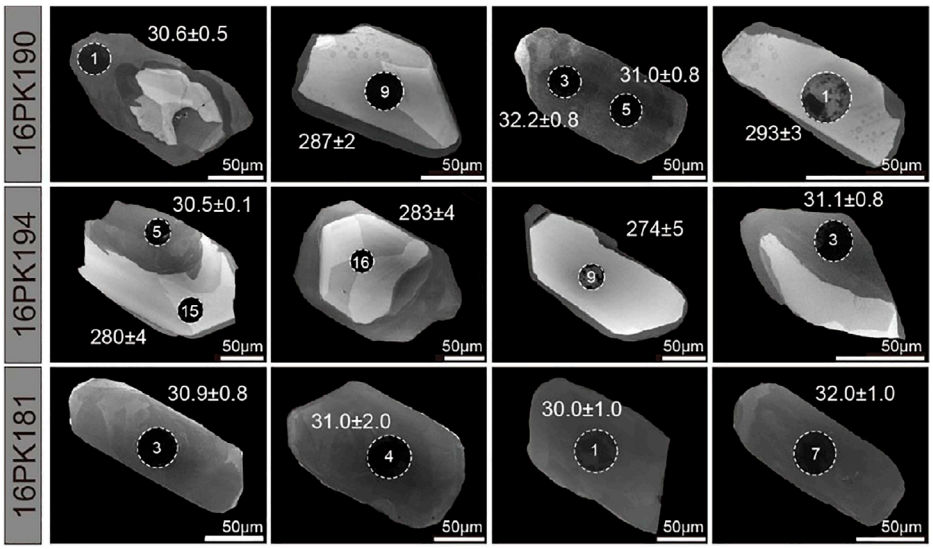

FIGURE 5 | Cathodoluminescence images of zircons from Stak samples. White digits are U-Pb ages, dashed cycles are analysis spots with analytical numbers. The age unit is Ma.

200 zircons of each sample were handpicked out from under a binocular microscope and mounted in epoxy resin together with zircon U-Pb age reference materials. Then the epoxy mounts were polished to expose the interior of the crystals. All grains were photographed in reflected and transmitted light under petrographic microscope to avoid fissures and inclusions. Cathodoluminescence (CL) and back-scattered electron (BSE) images were obtained using field emission scanning electron microscope (Nova NanoSEM 450) equipped with Gatan MomoCL4 at the Institute of Geology and Geophysics, Chinese Academy of Sciences (IGG-CAS). Mineral inclusions in zircon were identified using Raman spectroscopy at the IGG-CAS. Homogeneous zircons without inclusions or fissures were chosen for U-Pb dating and trace element analyses. Zircon U-Pb ages were determined by using secondary ion mass spectrometry (SIMS) and laser ablation-inductively coupled plasma-mass spectrometry (LA-ICP-MS). Zircon trace elements were acquired in the same run of age dating by LA-ICP-MS.

Secondary Ion Mass Spectrometry Zircon U-Pb Dating

Zircon U, Th, and Pb isotope analyses were performed with a Cameca IMS-1280HR SIMS at the IGG-CAS. Detailed instrumental parameters and analytical procedures are described by Li et al. (2009). The analytical spot is about 20×30 μm in size. Plešovice zircon standard ($^{206}Pb/^{238}U$ age of 337.3 Ma; Sláma et al., 2008) was interspersed with unknown grains. Nonradiogenic ^{204}Pb was used for common Pb correction of measured compositions, and the present-day crustal common Pb composition is used in the model of Stacey and Kramers (1975). An inhouse zircon standard Qinghu was alternately analyzed together with other unknown zircons for the purpose of monitoring external uncertainties of SIMS U-Pb zircon dating calibrated by the Plešovice standard. Excel and the add-in Isoplot 2.49 program (Ludwig, 2001) were used for data calculation. Uncertainties on individual analyses in **Supplementary Table S3** are reported at 1σ level. The weighted mean U-Pb ages are quoted with 95% confidence interval. Seven measurements on Qinghu zircon yielded a Concordia age of 159.7 ± 1.8 Ma, which is identical within errors with the recommended value of 159.5 ± 0.2 Ma (Li et al., 2013).

Laser Ablation-Inductively Coupled Plasma-Mass Spectrometry Zircon U-Pb Dating and Trace Element Analyses

U-Pb dating combined with *in situ* trace element analyses of zircons were carried out in a single run by Agilent 7500a ICP-MS instrument equipped with Geolas-193 UV laser ablation system at the State Key Laboratory of Continental Dynamics, Northwest University, China. Operating conditions and data processing are described by Liu et al. (2007) in detail. The spot diameter is 32 μm for two eclogites (16PK190 and 16PK196) and 44 μm for gneiss (16PK181) with a laser repetition rate of 6 Hz. Helium was used as the carrier gas. Laboratory standards (GJ-1, 91500, NIST 610) were interspersed with unknown grains. U-Th-Pb isotope ratios and trace element contents were calculated using the GLITTER 4.0 program (Macquarie University). Harvard zircon 91500 was used as external standard. To monitor the external uncertainties of U-Pb zircon dating calibrated against 91500, a second zircon standard GJ-1 was analyzed as an unknown together with other unknown zircons. Trace element concentrations were calibrated by using ^{29}Si as internal standard and NIST 610 as external standard. Data reduction was carried out using Isoplot/Excel version 2.49 (Ludwig, 2001). Fifteen measurements on GJ-1 and 32 measurements on 91500 yielded weighted mean $^{206}Pb/^{238}U$ ages of 602 ± 3.7 Ma (1σ) and 1,062.5 ± 2.8 Ma (1σ), respectively,

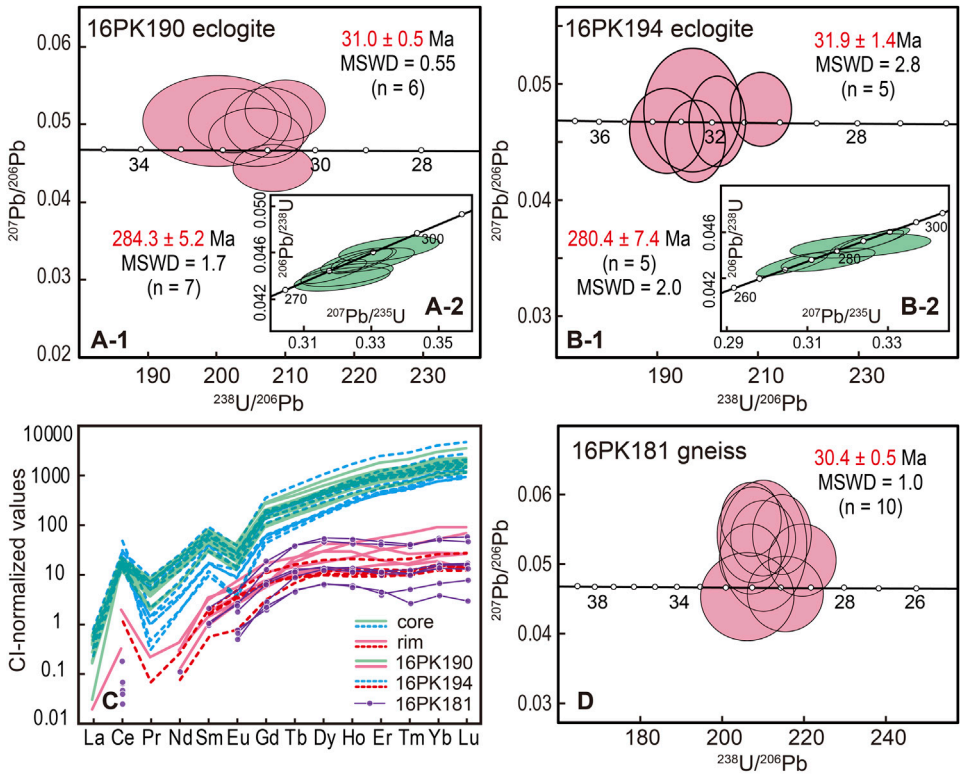

FIGURE 6 | Zircon U-Pb dates **(A,B,D)** and REE patterns **(C)**. **(A-1)**, **(B-1)**, **(D)** Tera-Wasserburg diagrams of metamorphic zircon U-Pb data uncorrected for common Pb. **(A-2)**, **(B-2)** Concordia diagrams for zircon cores of the Stak eclogites. **(C)** Chondrite-normalized REE patterns of zircons in the Stak samples. Chondrite data are from McDonough and Sun (1995). n, number of analyses; MSWD, mean square of weighted deviates.

which are in good agreement with the recommended value of 608 ± 0.4 Ma (Jackson et al., 2004) for GJ-1 and 1,065.4 ± 0.6 Ma (Wiedenbeck et al., 2004) for 91500.

RESULTS

The zircons from the two eclogites are mostly subhedral and consist of two major parts under cathodoluminescence (CL) images (**Figure 5**): 1) a core with relatively bright and slightly oscillatory zoning luminescence, and 2) a rim with relatively dark, homogeneous luminescence. Inclusions of diopside, amphibole, plagioclase, quartz, and apatite are common in the zircon cores, while the rims have garnet, rutile, and quartz inclusions without plagioclase and coesite (**Supplementary Figure S1**). Fourteen zircons from sample 16PK190 and 10 zircons from sample 16PK194 were dated by the SIMS method. The Th/U ratios of the zircon cores and rims are 2.05–3.17 and ≤0.05, respectively (**Supplementary Table S3**). The SIMS dating results show that the two eclogites, 16PK190 and 16PK194, have similar $^{206}Pb/^{238}U$ weighted mean ages of 284.3 ± 5.2 Ma (MSWD = 1.7, $n = 7$) and 280.4 ± 7.4 Ma (MSWD = 2.0, $n = 5$) for the zircon cores and 31.0 ± 0.5 Ma (MSWD = 0.55, $n = 6$), 31.9 ± 1.4 Ma (MSWD = 2.8, $n = 5$) for the zircon rims (**Figures 6A, B**). The LA-ICP-MS results (see the **Supplementary Figure S2**) are consistent with those of SIMS. The zircon cores have higher REE concentrations than the rims and are characterized by positive Ce anomalies, negative Eu anomalies, and steep heavy REE patterns (**Figure 6C**). The zircon rims for both samples show flat heavy REE patterns with a distinct lack of Eu anomalies (**Figure 6C**).

Zircons from the country gneiss 16PK181 are oval or prismatic crystals characterized by weak luminescence and patchy zoning under CL, with rare bright cores (**Figure 5**). All the analyses were conducted on the core-free zircons. They show low Th/U ratios (<0.01) (**Supplementary Table S3**) and REE concentrations (**Supplementary Table S5**), with flat heavy REE patterns and no negative Eu anomalies (**Figure 6C**). The SIMS dating result (30.4 ± 0.5 Ma, MSWD = 1.0, $n = 10$) (**Figure 6D**) is consistent with that of LA-ICP-MS (30.8 ± 0.8 Ma, MSWD = 0.46, $n = 7$) within errors (**Supplementary Figure S2**).

DISCUSSION

Timing of Eclogite-Facies Metamorphism

The $^{206}Pb/^{238}U$ weighted mean ages of ca. 284–280 Ma measured in the zircon cores from both eclogites represent the crystallization age of the magmatic protolith, which is demonstrated by their oscillatory zoning, high Th/U ratios, and steep REE patterns. This age is contemporaneous with the protolith formation of the Kaghan and Tso Morari UHP eclogites

(Rajkumar, 2015; Rehman et al., 2016), which is ascribed to the eruption of the Panjal Traps in the north Indian continental margin (Shellnutt, 2018). Our results, coupled with the similar whole-rock chemistry and Nd isotopic compositions between the Stak eclogites and the Panjal Traps volcanic rocks (Kouketsu et al., 2017), indicate that the western Himalayan eclogites likely shared the same protoliths during the Permian magmatism of the Panjal Traps.

The rims of the eclogite zircons exhibit metamorphic characteristics and equilibrium texture with HP phases. The date of ca. 31 Ma most likely reflects eclogite-facies zircon recrystallization because, 1) the zircon rims have inclusions of garnet and rutile without plagioclase, 2) the disequilibrium texture of zircon with symplectitic diopside and plagioclase implies zircon inclusions presented in preexisting omphacite (**Figure 4**), and 3) the REE data indicate recrystallization in the presence of garnet and absence of plagioclase (**Figure 6C**). A similar metamorphic age (ca. 32 Ma) reported by Koukestsu et al. (2016) was interpreted as a recrystallization time after eclogite-facies metamorphism. However, the low Yb concentrations in those zircons only reflect equilibration with garnet, which could occur both under eclogite- and granulite-facies conditions. Moreover, metamorphic zircons from the country gneiss show REE characteristics and ages similar to those from the eclogites (**Figures 6C,D**). Therefore, the Stak massif was coherently buried beneath the Asian plate and underwent eclogite-facies metamorphism at ca. 31 Ma.

The HP metamorphic time of the Stak massif is at least 15 Ma later than the UHP metamorphic time (53–46 Ma) in the Kaghan and Tso Morari massifs (de Sigoyer et al., 2000; Kaneko et al., 2003; Donaldson et al., 2013). Therefore, the HP-UHP massifs in the western Himalaya were asynchronously buried to ~2.5–3.8 GPa, indicating a continuous subduction/collision process spanning more than 15 Ma. After the Kaghan and Tso Morari massifs experienced UHP metamorphism (~46 Ma) and rapid exhumation to the middle to lower crustal levels (~44–40 Ma) (de Sigoyer et al., 2000; Parrish et al., 2006; Wilke et al., 2010), the Stak massif was buried to HP eclogite-facie conditions at ca. 31 Ma. Such a continuous burial process recorded by HP–UHP rocks is common in other collisional belts such as Dabie-Sulu (e.g., Zhang et al., 2009), Alps (e.g., Berger and Bousquet, 2008), and the Western Gneiss Region (e.g., Kylander-Clark et al., 2009). In the following section, we will focus on how this process proceeded through time.

Implications for change in subduction dip angle through time

The HP metamorphism of the Stak massif is broadly contemporaneous with that of quartz eclogites, HP granulites, and garnet amphibolites (mostly 40–25 Ma) in the central and eastern Himalayas (**Figure 7A**) (Corrie et al., 2010; Zhang et al., 2010; Rubatto et al., 2013; Wang et al., 2021). This indicates that the subducted Indian continental slab probably underwent a coherent process along the Indus–Yarlung Suture Zone since 40 Ma. However, UHP metamorphism spatially restricted to the western Himalaya (Kaghan and Tso Morari) was only recognized

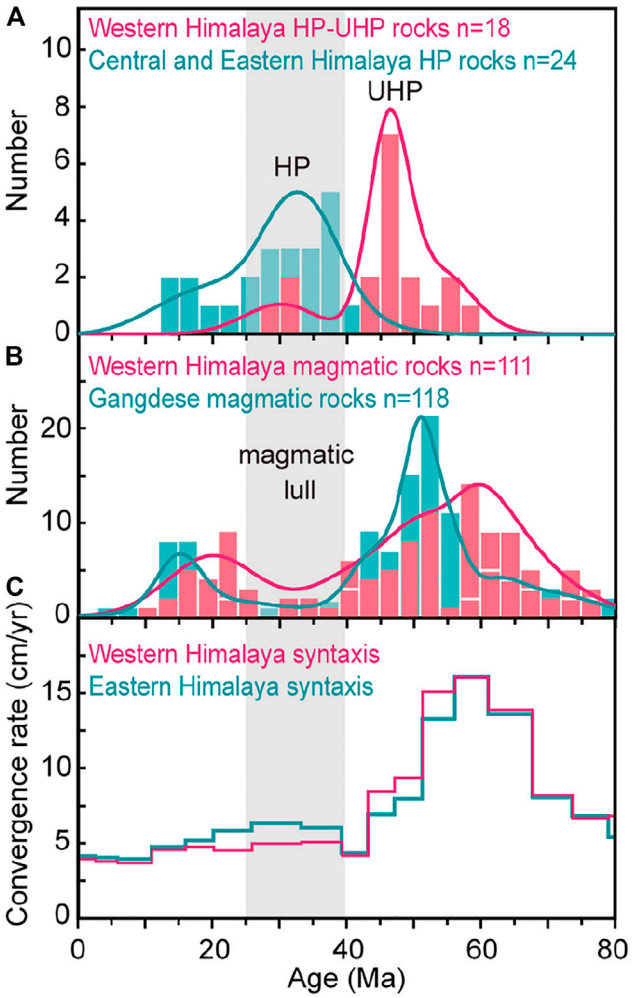

FIGURE 7 | (A) Cumulative probability curve and histogram showing the peak metamorphic ages of the HP and UHP rocks in the western (red) and central-eastern Himalayas (green). **(B)** Cumulative probability curve and histogram for the crystallization ages of the western Himalaya (South Karakoram, Kohistan–Ladakh Arc, red), and Gangdese (green) magmatic rocks. **(C)** India–Asia convergence rates. Detailed data and sources are listed in **Supplementary Table S6**.

before ca. 46 Ma (Kaneko et al., 2003; Donaldson et al., 2013). The discrepancy of HP–UHP timing in the western and central Himalayas could be induced by continental subduction of a jagged Indian margin (Guillot et al., 2008), by different exhumation styles (residence times at crustal level) of eclogites (O'Brien, 2019; Rehman, 2019), or by changes in subduction dip angle (**Figure 2**). However, it is unlikely that an irregular northern margin of India would trigger the long discrepancy (>15 Ma) between UHP and HP peak metamorphic ages. The different *P-T*-t paths observed between UHP and HP eclogites were interpreted to result from the prolonged residence times in the central and eastern Himalayas but rapid exhumation of UHP rocks in the west (Rehman, 2019). However, the different exhumation styles are not the first-order mechanism responsible for the distinct peak metamorphic ages of

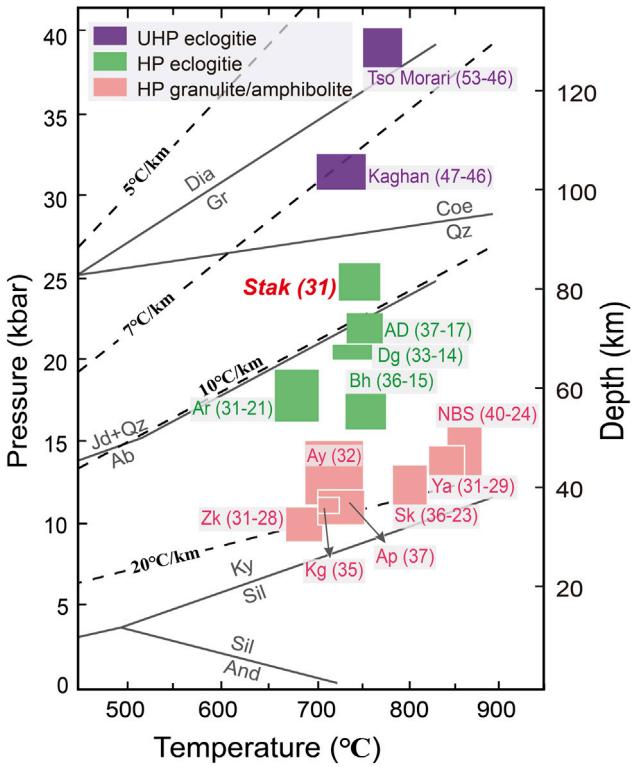

FIGURE 8 | Integrated peak *P-T* conditions and ages of eclogites and HP granulites in the Himalayan orogen. The age data sources are listed in **Supplementary Table S6**. Source references for *P-T* conditions: Annapurna (Ap) (Kohn and Corrie, 2011), Ama Drime (AD) (Li et al., 2018), Arun (Ar) (Corrie et al., 2010), Ayilari (Ay) (Chen et al., 2021), Bhutan (Bh) (Grujic et al., 2011), Dinggye (Dg) (Wang et al., 2017), Kaghan (Kaneko et al., 2003), Sikkim (Sk) (Faak et al., 2012), Stak (Lanari et al., 2013), Tso Morari (Mukherjee et al., 2005), Yadong (Ya) (Zhang et al., 2017), Namche Barwa Syntaxis (NBS) (Zhang et al., 2015), and Zanskar (Zk) (Vance and Harris, 1999).

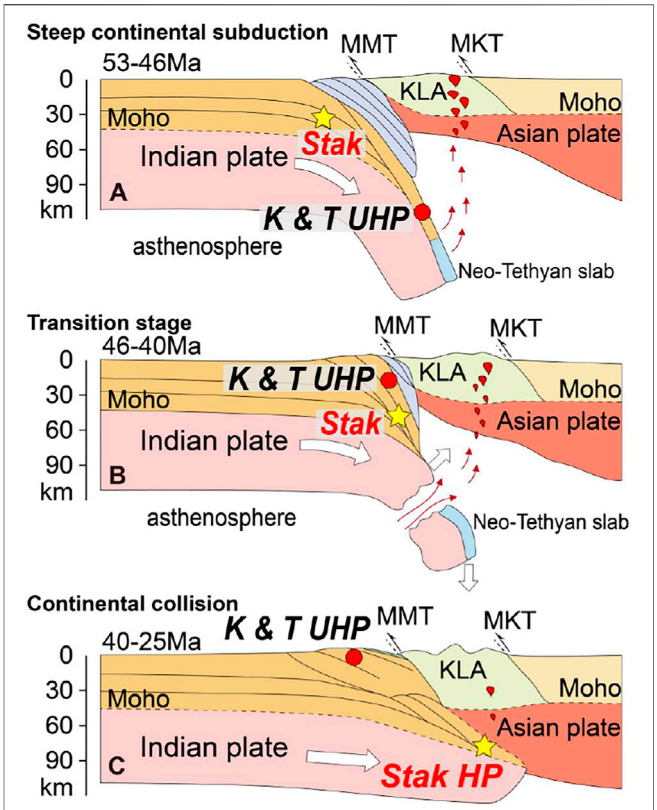

FIGURE 9 | Schematic diagrams illustrating the evolution process of the western Himalaya during the India–Asia collision. **(A)** Steep subduction and UHP metamorphism of the Indian continental slab at ca. 53–46 Ma. **(B)** Breakoff of the Neo-Tethyan lithosphere induced fast exhumation of UHP metamorphic rocks and then rebound of subducted Indian continental slab at ca. 46–40 Ma. **(C)** Continuous (ca. 40–25 Ma) low-angle underthrusting of the Indian continental slab during collision contributed to the HP metamorphism and magmatic lull. K & T, Kaghan and Tso Morari; KLA, Kohistan–Ladakh arc.

HP–UHP rocks. The ~31 Ma eclogite-facies metamorphic age in Stak is similar to those recorded in the central Himalayan HP eclogite (~30 Ma; Wang et al., 2021) and the Zanskar HP granulite (31–28 Ma; Vance and Harris, 1999) and the Ayilari garnet amphibolite (~32 Ma; Chen et al., 2021) in the western Himalaya (**Figure 1B**), indicating that these HP rocks were synchronously buried to shallow depths much later than the UHP rocks.

Notably, the old UHP eclogites and young HP rocks record different peak-pressure thermal gradients (temperature change with depth, referred to as metamorphic *T/P*) (**Figure 8**), implying a change in the subduction geometry of the Indian continental slab during 46–40 Ma. The subduction of oceanic lithosphere (Neo-Tethys) after the initial India–Asia collision (~60 Ma; e.g., Parsons et al., 2020) would continuously release fluids or melts, generate convective corner flow in the mantle wedge, and, thus, induce magmatism at convergent plate margins (**Figure 7B**). The successive steep subduction of Indian continental crust driven by slab pull of the Neo-Tethys underwent UHP metamorphism (low *T/P*) at 53–46 Ma (**Figures 2A** and **9A**). The steep subduction of the Indian continental slab is also supported by the presence of the UHP eclogite units in the western Himalaya now directly adjacent to the Indus–Tsangpo suture zone (O'Brien, 2019). However, after ~40 Ma, the sole occurrence of HP metamorphism (high *T/P*) along the strike reflects an increase of geothermal gradient that requires a change in subduction dip angle (**Figures 2B** and **9B**). These young HP rocks most likely resulted from low-angle underthrusting during continental collision (Guillot et al., 2008; Soret et al., 2021). Therefore, the change in subduction dip angle of the Indian continental slab during 46–40 Ma is critical for the transition from continental subduction to collision dynamics.

The change in subduction dip angle can be induced by the continuous subduction of buoyant continental lithosphere (Parsons et al., 2021) or by the breakoff of the oceanic (Neo-Tethyan) lithosphere (Davies and von Blanckenburg, 1995; Magni et al., 2017). Breakoff of the Neo-Tethyan lithosphere would lead to fast exhumation of UHP rocks (Kohn and Parkinson, 2002), uplifting of the buoyant continental lithosphere, and shifting to gently dipping subduction or underthrusting (Davies and von Blanckenburg, 1995;

Chemenda et al., 2000). In addition, slab breakoff mostly occurs at greater depths (~130–240 km) than the base of the overriding lithosphere and would not trigger significant magmatism at convergent margins (e.g., Freeburn et al., 2017), which is consistent with the weak magmatism within the Asian plate at 46–40 Ma (**Figure 7B**). There are many lines of evidence supporting the breakoff of the Neo-Tethyan slab around 46–40 Ma after the initial India–Asia collision. 1) According to paleomagnetic reconstructions and tomographical observations, Negredo et al. (2007) estimated the breakoff of oceanic slab occurring at 48–44 Ma. 2) The rapid exhumation of the Kaghan UHP eclogite from ~100 to ~35 km during 46–44 Ma (Parrish et al., 2006) also agrees with the breakoff model (Kohn and Parkinson, 2002). 3) Based on tomography, the Asian tectonics reconstructions and the Indian plate kinematics, Replumaz et al. (2014) proposed that the major breakoff between India and the Tethys ocean occurred at ~45 Ma. However, Parsons et al. (2021) proposed a different timing for slab breakoff based on interpretations of the same tomographic anomalies. 4) The occurrence of 42–40 Ma intraplate-type mafic dykes in eastern Tibet supports the breakoff of subducting Neo-Tethyan slab from the Indian continental slab during the middle Eocene (Xu et al., 2008). 5) The 45 Ma oceanic island basalt-type gabbro in southern Tibet was used to constrain the breakoff time of the Neo-Tethyan slab (Ji et al., 2016). Numerical studies suggest that the timing of slab breakoff after the onset of continental collision varies from 10 to 25 Ma, which is largely affected by the strength and age of the subducting oceanic slab (e.g., van Hunen and Allen, 2011). Our proposed slab breakoff timing (46–40 Ma) for the old Neo-Tethyan slab after the onset of continental collision (~60 Ma) broadly fits this modeled result. Therefore, we suggest that the different *T/P* and ages between the Himalayan UHP and HP rocks were induced by the breakoff of the Neo-Tethyan slab and subsequent transition from steep continental subduction to low-angle underthrusting (collision) at 46–40 Ma (**Figure 9B**).

The synchronous HP metamorphism induced by laterally large-scale low-angle underthrusting is also supported by palaeomagnetic and magmatic data. Since the Late Cretaceous, the India–Asia convergence rates in the eastern and western Himalayas show high consistency (**Figure 7C**), decreasing from 140–160 to 80–100 mm/year at 52–50 Ma and then decreasing to 40–60 mm/year at ca. 45 Ma (van Hinsbergen et al., 2011). The first deceleration is attributed to the initial India–Asia collision (van Hinsbergen et al., 2011), whereas the second most likely resulted from the loss of oceanic slab pull after breakoff (e.g., Bercovici et al., 2015; Ji et al., 2016) or the India–Asia second collision (45–40 Ma) after an earlier collision (~60 Ma) of either Indian continent + intraoceanic arc or greater India microcontinent + Asia (e.g., Parsons et al., 2020, 2021). A low convergence rate benefits sufficient heat exchange between the subducting plate and the overlying mantle, thus inducing HP metamorphism with high *T*/*P* (Guillot et al., 2008). In addition, the Himalayan magmatic activities from east to west were systematically complementary to the HP metamorphic events after 40 Ma. The Kohistan–Ladakh–Gangdese arc system and south Karakoram exhibit a coherent magmatic lull at 40–25 Ma (**Figure 7B**). The Stak eclogite in the western Himalaya and most of the other HP rocks in the central and eastern Himalaya also formed at this stage (**Figures 7A** and **9C**). The low-angle underthrusting after slab breakoff would have driven the asthenosphere beneath the Asian plate away and then shielded the active continental margin from convective heat, which would have led to the magmatic lull in the convergent margin (Chung et al., 2005; Ji et al., 2016; Ji et al., 2020). The driving force for the continuous convergence and underthrusting after the breakoff of the Neo-Tethyan slab could be subduction of Australian oceanic lithosphere (e.g., Parsons et al., 2021) or subduction of Indian continental lithosphere (e.g., Capitanio et al., 2010). In addition, the continuous low-angle underthrusting during continental collision at 40–25 Ma potentially enhanced crustal thickening (Soret et al., 2021) and elevated the thermal structure of orogenic wedge due to radiogenic heat production in the thickened crust (Berger et al., 2011), contributing to the high- or ultrahigh-temperature overprints in HP eclogites during exhumation (Wang et al., 2021). In this regard, the change in subduction dip angle of continental slab would have influenced both magmatic activities and peak geothermal gradients of HP–UHP rocks. To summarize, a lateral (>2,500 km) change in the subduction geometry of the Indian continental slab during the middle Eocene would be broadly consistent with the igneous and metamorphic records.

CONCLUSION

The Stak eclogites and their country gneiss in the western Himalayan syntexis provide insight into the change in subduction dip angle of the Indian continental lithosphere. Precise geochronological data show that the Stak massif underwent HP eclogite-facie metamorphism at ~31 Ma, which is at least ~15 Ma later than the Himalayan UHP metamorphism. Considering the discrepancies in peak ages and geothermal gradients between the Himalayan HP and UHP metamorphic rocks, we suggest that the Indian continental lithosphere underwent a coherent change in subduction dip angle during 46–40 Ma. Based on geological and geophysical evidence, this change in subduction geometry is likely induced by the breakoff of the Neo-Tethyan slab. We suggest that the change in subduction dip angle is a critical process controlling the transition from continental subduction to collision dynamics.

DATA AVAILABILITY STATEMENT

The original contributions presented in the study are included in the article/**Supplementary Materials**. Further inquiries can be directed to the corresponding author.

AUTHOR CONTRIBUTIONS

SC, YC, and QL performed the analyses. SC contributed to the data sorting and compilation. YC interpreted the data. YC, SC, and SG wrote the manuscript.

FUNDING

This work is financially supported by the National Natural Science Foundation of China (Nos. 41822202 and 41490614).

ACKNOWLEDGMENTS

We thank Profs. Lin Ding, Weiming Fan, Junmeng Zhao, Jamie Cutts, and Fulong Cai, Muhammad Qasim, Lin Chen, and Weiqiang Ji for inspiring discussion and constructive comments. D. Zhang, X.X. Ling, and C.R. Diwu are thanked for their help during the electron probe microanalysis, SIMS, and LA-ICP-MS analyses. Critical reviews by Andy Parsons and Xiao-Ping Xia and editorial handling by Oliver Jagoutz and Valerio Acocella helped to improve the manuscript.

SUPPLEMENTARY MATERIAL

The Supplementary Material for this article can be found online at: https://www.frontiersin.org/articles/10.3389/feart.2021.790999/full#supplementary-material

REFERENCES

Bercovici, D., Schubert, G., and Ricard, Y. (2015). Abrupt Tectonics and Rapid Slab Detachment with Grain Damage. *Proc. Natl. Acad. Sci. USA* 112 (5), 1287–1291. doi:10.1073/pnas.1415473112

Berger, A., and Bousquet, R. (2008). Subduction-related Metamorphism in the Alps: Review of Isotopic Ages Based on Petrology and Their Geodynamic Consequences. *Geol. Soc. Lond. Spec. Publications* 298, 117–144. doi:10.1144/SP298.7

Berger, A., Schmid, S. M., Engi, M., Bousquet, R., and Wiederkehr, M. (2011). Mechanisms of Mass and Heat Transport during Barrovian Metamorphism: A Discussion Based on Field Evidence from the Central Alps (Switzerland/northern Italy). *Tectonics* 30 (1). doi:10.1029/2009TC002622

Capitanio, F. A., Morra, G., Goes, S., Weinberg, R. F., and Moresi, L. (2010). India-asia Convergence Driven by the Subduction of the Greater Indian Continent. *Nat. Geosci* 3 (2), 136–139. doi:10.1038/ngeo725

Chemenda, A. I., Burg, J. P., and Mattauer, M. (2000). Evolutionary Model of the Himalaya-Tibet System: Geopoem: Based on New Modelling, Geological and Geophysical Data. *Earth Planet. Sci. Lett.* 174 (3–4), 397–409. doi:10.1016/S0012-821X(99)00277-0

Chen, X., Schertl, H.-P., Gu, P., Zheng, Y., Xu, R., Zhang, J., et al. (2021). Newly Discovered MORB-type HP Garnet Amphibolites from the Indus-Yarlung Tsangpo Suture Zone: Implications for the Cenozoic India-Asia Collision. *Gondwana Res.* 90, 102–117. doi:10.1016/j.gr.2020.11.006

Corrie, S. L., Kohn, M. J., and Vervoort, J. D. (2010). Young Eclogite from the Greater Himalayan Sequence, Arun Valley, Eastern Nepal: *P-T*-t Path and Tectonic Implications. *Earth Planet. Sci. Lett.* 289 (3–4), 406–416. doi:10.1016/j.epsl.2009.11.029

Davies, J. H., and von Blanckenburg, F. (1995). Slab Breakoff: a Model of Lithosphere Detachment and its Test in the Magmatism and Deformation of Collisional Orogens. *Earth Planet. Sci. Lette* . 129 (1–4), 85–102. doi:10.1016/0012-821X(94)00237-S

de Sigoyer, J., Chavagnac, V., Blichert-Toft, J., Villa, I. M., Luais, B., Guillot, S., et al. (2000). Dating the Indian continental Subduction and Collisional Thickening in the Northwest Himalaya: Multichronology of the Tso Morari Eclogites. *Geology* 28 (6), 487–490. doi:10.1130/0091-7613(2000)28<487:DTICSA>2.0.CO;2

Ding, H., Zhang, Z., Dong, X., Tian, Z., Xiang, H., Mu, H., et al. (2016a). Early Eocene (C . 50 Ma) Collision of the Indian and Asian Continents: Constraints from the North Himalayan Metamorphic Rocks, southeastern Tibet. *Earth Planet. Sci. Lett.* 435, 64–73. doi:10.1016/j.epsl.2015.12.006

Ding, H., Zhang, Z., Hu, K., Dong, X., Xiang, H., and Mu, H. (2016b). *P-T*-t-D Paths of the North Himalayan Metamorphic Rocks: Implications for the Himalayan Orogeny. *Tectonophysics* 683, 393–404. doi:10.1016/j.tecto.2016.06.035

Donaldson, D. G., Webb, A. A. G., Menold, C. A., Kylander-Clark, A. R. C., and Hacker, B. R. (2013). Petrochronology of Himalayan Ultrahigh-Pressure Eclogite. *Geology* 41 (8), 835–838. doi:10.1130/g33699.1

Duretz, T., and Gerya, T. V. (2013). Slab Detachment during continental Collision: Influence of Crustal Rheology and Interaction with Lithospheric Delamination. *Tectonophysics* 602, 124–140. doi:10.1016/j.tecto.2012.12.024

Faak, K., Chakraborty, S., and Dasgupta, S. (2012). Petrology and Tectonic Significance of Metabasite Slivers in the Lesser and Higher Himalayan Domains of Sikkim, India. *J. Metamorph. Geol.* 30 (6), 599–622. doi:10.1111/j.1525-1314.2012.00987.x

Freeburn, R., Bouilhol, P., Maunder, B., Magni, V., and van Hunen, J. (2017). Numerical Models of the Magmatic Processes Induced by Slab Breakoff. *Earth Planet. Sci. Lett.* 478, 203–213. doi:10.1016/j.epsl.2017.09.008

Grujic, D., Warren, C. J., and Wooden, J. L. (2011). Rapid Synconvergent Exhumation of Miocene-Aged Lower Orogenic Crust in the Eastern Himalaya. *Lithosphere* 3 (5), 346–366. doi:10.1130/L154.1

Guillot, S., Mahéo, G., de Sigoyer, J., Hattori, K. H., and Pêcher, A. (2008). Tethyan and Indian Subduction Viewed from the Himalayan High- to Ultrahigh-Pressure Metamorphic Rocks. *Tectonophysics* 451 (1–4), 225–241. doi:10.1016/j.tecto.2007.11.059

Hazarika, D., Wadhawan, M., Paul, A., Kumar, N., and Borah, K. (2017). Geometry of the Main Himalayan Thrust and Moho beneath Satluj valley, Northwest Himalaya: Constraints from Receiver Function Analysis. *J. Geophys. Res. Solid Earth* 122 (4), 2929–2945. doi:10.1002/2016jb013783

Jackson, S. E., Pearson, N. J., Griffin, W. L., and Belousova, E. A. (2004). The Application of Laser Ablation-Inductively Coupled Plasma-Mass Spectrometry to *In Situ* U-Pb Zircon Geochronology. *Chem. Geology.* 211 (1–2), 47–69. doi:10.1016/j.chemgeo.2004.06.017

Ji, W.-Q., Wu, F.-Y., Chung, S.-L., Wang, X.-C., Liu, C.-Z., Li, Q.-L., et al. (2016). Eocene Neo-Tethyan Slab Breakoff Constrained by 45 Ma Oceanic Island basalt-type Magmatism in Southern Tibet. *Geology* 44 (4), 283–286. doi:10.1130/g37612.1

Ji, W.-Q., Wu, F.-Y., Wang, J.-M., Liu, X.-C., Liu, Z.-C., Zhang, Z., et al. (2020). Early Evolution of Himalayan Orogenic belt and Generation of Middle Eocene Magmatism: Constraint from Haweng Granodiorite Porphyry in the Tethyan Himalaya. *Front. Earth Sci.* 8, 236. doi:10.3389/feart.2020.00236

Kaneko, Y., Katayama, I., Yamamoto, H., Misawa, K., Ishikawa, M., Rehman, H. U., et al. (2003). Timing of Himalayan Ultrahigh-Pressure Metamorphism: Sinking Rate and Subduction Angle of the Indian continental Crust beneath Asia. *J. Metamorph. Geol.* 21 (6), 589–599. doi:10.1046/j.1525-1314.2003.00466.x

Kay, S. M., and Coira, B. L. (2009). "Shallowing and Steepening Subduction Zones, continental Lithospheric Loss, Magmatism, and Crustal Flow under the Central Andean Altiplano-Puna Plateau," in *Backbone of the Americas: Shallow Subduction, Plateau Uplift, and Ridge and Terrane Collision*. Editors S. M. Kay, V. A. Ramos, and W. R. Dickinson (New York: Geol Soc Am Mem), 204, 229–259. doi:10.1130/2009.1204(11)

Kohn, M. J., and Corrie, S. L. (2011). Preserved Zr-Temperatures and U-Pb Ages in High-Grade Metamorphic Titanite: Evidence for a Static Hot Channel in the Himalayan Orogen. *Earth Planet. Sci. Lett.* 311 (1–2), 136–143. doi:10.1016/j.epsl.2011.09.008

Kohn, M. J., and Parkinson, C. D. (2002). Petrologic Case for Eocene Slab Breakoff during the Indo-Asian Collision. *Geol* 30 (7), 591–594. doi:10.1130/0091-7613(2002)030<0591:pcfesb>2.0.co;2

Kouketsu, Y., Hattori, K., and Guillot, S. (2017). Protolith of the Stak Eclogite in the Northwestern Himalaya. *Ijg* 136 (1), 64–72. doi:10.3301/IJG.2015.41

Kouketsu, Y., Hattori, K., Guillot, S., and Rayner, N. (2016). Eocene to Oligocene Retrogression and Recrystallization of the Stak Eclogite in Northwest Himalaya. *Lithos* 240-243, 155–166. doi:10.1016/j.Lithos.2015.10.022

Kylander-Clark, A. R. C., Hacker, B. R., Johnson, C. M., Beard, B. L., and Mahlen, N. J. (2009). Slow Subduction of a Thick Ultrahigh-Pressure Terrane. *Tectonics* 28, a–n. doi:10.1029/2007TC002251

Lanari, P., Riel, N., Guillot, S., Vidal, O., Schwartz, S., Pêcher, A., et al. (2013). Deciphering High-Pressure Metamorphism in Collisional Context Using Microprobe Mapping Methods: Application to the Stak Eclogitic Massif (Northwest Himalaya). *Geology* 41 (2), 111–114. doi:10.1130/G33523.1

Le Fort, P., Guillot, S., and Pêcher, A. (1997). HP Metamorphic belt along the Indus Suture Zone of NW Himalaya: New Discoveries and Significance. *Comptes Rendus de l'Académie des Sci. - Ser. IIA - Earth Planet. Sci.* 325 (10), 773–778. doi:10.1016/S1251-8050(97)82755-3

Li, Q., Zhang, L., Fu, B., Bader, T., and Yu, H. (2018). Petrology and Zircon U-Pb Dating of Well-preserved Eclogites from the Thongmön Area in central Himalaya and Their Tectonic Implications. *J. Metamorph. Geol.* 37 (2), 203–226. doi:10.1111/jmg.12457

Li, X.-H., Li, W.-X., Li, Z.-X., Lo, C.-H., Wang, J., Ye, M.-F., et al. (2009). Amalgamation between the Yangtze and Cathaysia Blocks in South China: Constraints from SHRIMP U-Pb Zircon Ages, Geochemistry and Nd-Hf Isotopes of the Shuangxiwu Volcanic Rocks. *Precambrian Res.* 174 (1-2), 117–128. doi:10.1016/j.precamres.2009.07.004

Li, X., Tang, G., Gong, B., Yang, Y., Hou, K., Hu, Z., et al. (2013). Qinghu Zircon: A Working Reference for Microbeam Analysis of U-Pb Age and Hf and O Isotopes. *Chin. Sci. Bull.* 58 (36), 4647–4654. doi:10.1007/s11434-013-5932-x

Liu, X., Gao, S., Diwu, C., Yuan, H., and Hu, Z. (2007). Simultaneous *In-Situ* Determination of U-Pb Age and Trace Elements in Zircon by LA-ICP-MS in 20 μm Spot Size. *Chin. Sci Bull* 52 (9), 1257–1264. doi:10.1007/s11434-007-0160-x

Ludwig, K. (2001). Users Manual for Isoplot/Ex Rev. 2.49: A Geochronological Toolkit for Microsoft Excel. *Calif. Berkeley Geochronol. Cent. Spec. Publ.* 1 (1), 56.

Magni, V., Allen, M. B., van Hunen, J., and Bouilhol, P. (2017). Continental Underplating after Slab Break-Off. *Earth Planet. Sci. Lett.* 474, 59–67. doi:10.1016/j.epsl.2017.06.017

McDonough, W. F., and Sun, S. -S. (1995). The Composition of the Earth. *Chem.Geol.* 120 (3–4), 223–253. doi:10.1016/0009-2541(94)00140-4

Mukheerjee, B., Sachan, H., and Ahmad, T. (2005). A New Occurrence of Microdiamond from Indus Suture Zone, Himalata: a Possible Origin. *Spec. Ext Abstrgéol Alp.* 44, 136.

Negredo, A. M., Replumaz, A., Villaseñor, A., and Guillot, S. (2007). Modeling the Evolution of continental Subduction Processes in the Pamir-Hindu Kush Region. *Earth Planet. Sci. Lett.* 259, 212–225. doi:10.1016/j.epsl.2007.04.043

O'Brien, P. J. (2019). Tso Morari Coesite Eclogite: Pseudosection Predictions V. The Preserved Record and Implications for Tectonometamorphic Models. *Geol. Soc. Lond. Spec. Publications* 474 (1), 5–24. doi:10.1144/SP474.16

O'Brien, P. J., Zotov, N., Law, R., Khan, M. A., and Jan, M. Q. (2001). Coesite in Himalayan Eclogite and Implications for Models of India-Asia Collision. *Geology* 29 (5), 352–438. doi:10.1130/0091-7613(2001)029<0435:CIHEAI>2.0.CO10.1130/0091-7613(2001)029<0435:ciheai>2.0.co;2

Parrish, R. R., Gough, S. J., Searle, M. P., and Waters, D. J. (2006). Plate Velocity Exhumation of Ultrahigh-Pressure Eclogites in the Pakistan Himalaya. *Geol* 34 (11), 989–992. doi:10.1130/G22796A.1

Parsons, A. J., Hosseini, K., Palin, R. M., and Sigloch, K. (2020). Geological, Geophysical and Plate Kinematic Constraints for Models of the India-Asia Collision and the post-Triassic central Tethys Oceans. *Earth-Science Rev.* 208, 103084. doi:10.1016/j.earscirev.2020.103084

Parsons, A. J., Sigloch, K., and Hosseini, K. (2021). Australian Plate Subduction Is Responsible for Northward Motion of the India-Asia Collision Zone and ~1,000 Km Lateral Migration of the Indian Slab. *Geophys. Res. Lett.* 48, e2021GL094904. doi:10.1029/2021gl094904

Paterson, S. R., and Ducea, M. N. (2015). Arc Magmatic Tempos: Gathering the Evidence. *Elements* 11 (2), 91–98. doi:10.2113/gselements.11.2.91

Rajkumar, A. (2015). *Prograde Histories in High-P to Ultra-high-P Metamorphic Rocks from Tibet and Northern India*. Ph.D. thesis. Sydney: The University of Sydney.

Rehman, H. U. (2019). Geochronological enigma of the HP-UHP Rocks in the Himalayan Orogen. *Geol. Soc. Lond. Spec. Publications* 474 (1), 183–207. doi:10.1144/SP474.14

Rehman, H. U., Lee, H.-Y., Chung, S.-L., Khan, T., O'Brien, P. J., and Yamamoto, H. (2016). Source and Mode of the Permian Panjal Trap Magmatism: Evidence from Zircon U-Pb and Hf Isotopes and Trace Element Data from the Himalayan Ultrahigh-Pressure Rocks. *Lithos* 260, 286–299. doi:10.1016/j.lithos.2016.06.001

Replumaz, A., Capitanio, F. A., Guillot, S., Negredo, A. M., and Villaseñor, A. (2014). The Coupling of Indian Subduction and Asian continental Tectonics. *Gondwana Res.* 26, 608–626. doi:10.1016/j.gr.2014.04.003

Riel, N., Hattori, K., Guillot, S., Rayner, N., Davis, B., Latif, M., et al. (2008). SHRIMP Zircon Ages of Eclogites in the Stak Massif, Northern Pakistan. *Himalayan J. Sci.* 5, 119–120. doi:10.3126/hjs.v5i7.1307

Rubatto, D., Chakraborty, S., and Dasgupta, S. (2013). Timescales of Crustal Melting in the Higher Himalayan Crystallines (Sikkim, Eastern Himalaya) Inferred from Trace Element-Constrained Monazite and Zircon Chronology. *Contrib. Mineral. Petrol.* 165 (2), 349–372. doi:10.1007/s00410-012-0812-y

Sachan, H. K., Mukherjee, B. K., Ogasawara, Y., Maruyama, S., Ishida, H., Muko, A., et al. (2004). Discovery of Coesite from Indus Suture Zone (ISZ), Ladakh, India: Evidence for Deep Subduction. *ejm* 16 (2), 235–240. doi:10.1127/0935-1221/2004/0016-0235

Shellnutt, J. G. (2018). The Panjal Traps. *Geol. Soc. Lond. Spec. Publications* 463, 59–86. doi:10.1144/SP463.4

Sláma, J., Košler, J., Condon, D. J., Crowley, J. L., Gerdes, A., Hanchar, J. M., et al. (2008). Plešovice Zircon - A New Natural Reference Material for U-Pb and Hf Isotopic Microanalysis. *Chem. Geology.* 249 (1–2), 1–35. doi:10.1016/j.chemgeo.2007.11.005

Soret, M., Larson, K. P., Cottle, J., and Ali, A. (2021). How Himalayan Collision Stems from Subduction. *Geology* 49, 894–898. doi:10.1130/G48803.1

St-Onge, M. R., Rayner, N., Palin, R. M., Searle, M. P., and Waters, D. J. (2013). Integrated Pressure-Temperature-Time Constraints for the Tso Morari Dome (Northwest India): Implications for the Burial and Exhumation Path of UHP Units in the Western Himalaya. *J. Meta. Geol.* 31 (5), 469–504. doi:10.1111/jmg.12030

Stacey, J. S., and Kramers, J. D. (1975). Approximation of Terrestrial lead Isotope Evolution by a Two-Stage Model. *Earth Planet. Sci. Lett.* 26 (2), 207–221. doi:10.1016/0012-821X(75)90088-6

van Hinsbergen, D. J. J., Steinberger, B., Doubrovine, P. V., and Gassmöller, R. (2011). Acceleration and Deceleration of India-Asia Convergence since the Cretaceous: Roles of Mantle Plumes and continental Collision. *J. Geophys. Res.* 116, B06101. doi:10.1029/2010jb008051

van Hunen, J., and Allen, M. B. (2011). Continental Collision and Slab Break-Off: A Comparison of 3-D Numerical Models with Observations. *Earth Planet. Sci. Lett.* 302, 27–37. doi:10.1016/j.epsl.2010.11.035

Vance, D., and Harris, N. (1999). Timing of Prograde Metamorphism in the Zanskar Himalaya. *Geol* 27 (5), 395–398. doi:10.1130/0091-7613(1999)027<0395:topmit>2.3.co;2

Wang, J.-M., Lanari, P., Wu, F.-Y., Zhang, J.-J., Khanal, G. P., and Yang, L. (2021). First Evidence of Eclogites Overprinted by Ultrahigh Temperature Metamorphism in Everest East, Himalaya: Implications for Collisional Tectonics on Early Earth. *Earth Planet. Sci. Lett.* 558, 116760. doi:10.1016/j.epsl.2021.116760

Wang, Y., Zhang, L., Zhang, J., and Wei, C. (2017). The Youngest Eclogite in central Himalaya: *P-T* Path, U-Pb Zircon Age and its Tectonic Implication. *Gondwana Res.* 41, 188–206. doi:10.1016/j.gr.2015.10.013

Whitney, D. L., and Evans, B. W. (2010). Abbreviations for Names of Rock-Forming Minerals. *Am. Mineral.* 95 (1), 185–187. doi:10.2138/am.2010.3371

Wiedenbeck, M., Hanchar, J. M., Peck, W. H., Sylvester, P., Valley, J., Whitehouse, M., et al. (2004). Further Characterisation of the 91500 Zircon crystal. *Geostand Geoanalyt Res.* 28 (1), 9–39. doi:10.1111/j.1751-908X.2004.tb01041.x

Wilke, F. D. H., O'Brien, P. J., Altenberger, U., Konrad-Schmolke, M., and Khan, M. A. (2010). Multi-stage Reaction History in Different Eclogite Types from the Pakistan Himalaya and Implications for Exhumation Processes. *Lithos* 114 (1–2), 70–85. doi:10.1016/j.lithos.2009.07.015

Wilke, F. D. H., O'Brien, P. J., Schmidt, A., and Ziemann, M. A. (2015). Subduction, Peak and Multi-Stage Exhumation Metamorphism: Traces from One Coesite-Bearing Eclogite, Tso Morari, Western Himalaya. *Lithos* 231, 77–91. doi:10.1016/j.lithos.2015.06.007

Xu, Y.-G., Lan, J.-B., Yang, Q.-J., Huang, X.-L., and Qiu, H.-N. (2008). Eocene Break-Off of the Neo-Tethyan Slab as Inferred from Intraplate-type Mafic

Dykes in the Gaoligong Orogenic belt, Eastern Tibet. *Chem. Geology.* 255, 439–453. doi:10.1016/j.chemgeo.2008.07.016

Yin, A. (2006). Cenozoic Tectonic Evolution of the Himalayan Orogen as Constrained by Along-Strike Variation of Structural Geometry, Exhumation History, and Foreland Sedimentation. *Earth-Science Rev.* 76 (1–2), 1–131. doi:10.1016/j.earscirev.2005.05.004

Zhang, R. Y., Liou, J. G., and Ernst, W. G. (2009). The Dabie-Sulu continental Collision Zone: A Comprehensive Review. *Gondwana Res.* 16, 1–26. doi:10.1016/j.gr.2009.03.008

Zhang, Z. M., Zhao, G. C., Santosh, M., Wang, J. L., Dong, X., and Liou, J. G. (2010). Two Stages of Granulite Facies Metamorphism in the Eastern Himalayan Syntaxis, South Tibet: Petrology, Zircon Geochronology and Implications for the Subduction of Neo-Tethys and the Indian Continent beneath Asia. *J. Metamorph. Geol.* 28 (7), . doi:10.1111/j.1525-1314.2010.00885.x

Zhang, Z., Xiang, H., Dong, X., Ding, H., and He, Z. (2015). Long-lived High-Temperature Granulite-Facies Metamorphism in the Eastern Himalayan Orogen, South Tibet. *Lithos* 212-215, 1–15. doi:10.1016/j.lithos.2014.10.009

Zhang, Z., Xiang, H., Dong, X., Li, W., Ding, H., Gou, Z., et al. (2017). Oligocene HP Metamorphism and Anatexis of the Higher Himalayan Crystalline Sequence in Yadong Region, East-central Himalaya. *Gondwana Res.* 41, 173–187. doi:10.1016/j.gr.2015.03.002

Conflict of Interest: The authors declare that the research was conducted in the absence of any commercial or financial relationships that could be construed as a potential conflict of interest.

The reviewer X-PX declared a past co-authorship with one of the authors, QL, to the handling editor.